Interaction of 80–164 MeV protons with nickel isotopes

M. E. Sadler,* P. P. Singh, and J. Jastrzebski†
Indiana University Cyclotron Facility, Bloomington, Indiana 47405

L. L. Rutledge, Jr.‡ and R. E. Segel
Northwestern University, Evanston, Illinois 60204

(Received 6 June 1979; revised manuscript received 19 February 1980)

Production cross sections of various final nuclei have been determined using the in-beam gamma rays produced during the 80, 100, 136, and 164 MeV proton bombardment of ^{58}Ni, ^{60}Ni, ^{62}Ni, and ^{64}Ni targets. From the systematics of these cross sections it is concluded that (a) typically, 1–2 nucleons are emitted in the fast pre-equilibrium phase leaving a few nuclei excited over a broad range of excitation energy, (b) the bulk of the final nuclei are produced following nucleon evaporation from the excited nuclear residues of the pre-equilibrium phase, (c) the fraction of the incident energy dissipated through fast emission increases from about 1/2 to 2/3 over the above energy range, (d) the average excitation energy of the nuclear residues of the pre-equilibrium phase is estimated to increase by only 10 MeV in going from about 40 to 50 MeV over the above energy range, and (e) no evidence is found for significantly preferred removal of alpha particles from the target nucleus. Detailed comparisons of the observed cross sections are made with the cascade and hybrid models. The cascade model yields better overall agreement with the measured results. A hybrid model which includes both multiple pre-equilibrium emission and geometric surface effects is needed if it is to be equally effective.

[NUCLEAR REACTIONS ^{58,60,62,64}Ni$(p,x\gamma)$, E_p=80, 100, 136, and 164 MeV; measured E_γ, σ_γ, σ production various final nuclei; results compared with cascade and hybrid exciton models including evaporation.]

I. INTRODUCTION

Historically, the mechanisms of nuclear reactions have been categorized in terms of (1) the direct processes, which occur on a time scale on the order of the time it takes the projectile to pass through the nucleus, and (2) the compound nuclear processes, which occur on a time scale many orders of magnitude greater than the direct processes and correspond to complete absorption of the projectile by the target from which a statistical decay (compound nucleus evaporation) of the system in equilibrium is assumed to ensue. The former is characterized, in particle emission spectra, by peaks near the beam energy corresponding to discrete and continuum states of the residual nucleus, and the latter by a broad hump at low energy, the shape and position of which can be described quite well by the statistical models. At the projectile energies greater than a few times the nuclear binding energies in the nucleus a third mechanism is recognized to play a significant role, namely that of "precompound" or "pre-equilibrium" emission. This is envisioned to correspond to a cascade of quasielastic nucleon-nucleon interactions in the nucleus and occurs on a time scale between those for direct and compound reactions as the projectile plus target nuclear system tends toward equilibrium.

Semiclassical models have been developed which embody few of the details of nuclear structure but employ more general properties of the interacting entities such as the mean free path of nucleons in nuclear matter derived from the free nucleon-nucleon scattering cross section suitably corrected for various effects, densities of particle-hole states at varying excitation, effects of the nuclear surface and emission rates of nucleons from a highly excited nuclear system. To some degree the existing and developing models can be categorized as "statistical" or "cascade." The former extends the statistical theory for compound nucleus emission to nonequilibrium systems and the latter considers successive intranuclear nucleon-nucleon collisions which produce a cascade of particles, using free nucleon-nucleon scattering cross sections modified to the nuclear environment. The calculated results obtained from each of these models are compared with experimentally observed quantities in this work to determine which, if any, of the models give a better description of reality and to find directions in which the models should be extended to bring them in accord with the observations.

The measurements presented here pertain to the determination of the production cross sections for residual final nuclei after targets of medium mass elements were bombarded by 80–164 MeV protons using the inclusive in-beam γ rays detected with

high resolution. These measurements are the first of a continuing program to decipher the broad features of the reaction mechanisms of proton-nucleus interactions in the 80 to 200 MeV proton energy domain. A preliminary report embodying the systematic trends of the observed cross sections and their implications has been published.[1] Complementary measurements of the recoil ranges of the residual nuclei[2] of the γ-ray multiplicities of the residual nuclei[3] and of the differential cross sections of the charged particles[4] have been completed and shall be published elsewhere.

It is appropriate to list here some of the motivations which led to the initiation of this experimental program. Earlier measurements of this type,[5-11] primarily with proton and pion beams, reported enhanced production of residual nuclei which were an integral number of alpha particles removed from the target, thus focusing interest on the role of direct multiple alpha knockout in the reaction process. Furthermore, previously reported production cross sections at 100 MeV[10] with ^{58}Ni were systematically lower by a factor of 2 with respect to those reported at 200 MeV.[11] This difference was hard to understand in terms of the expected energy dependence of the cross sections. Detailed measurements in the 80–200 MeV energy range have not only helped to clear some of the above discrepancies[1] but also have provided systematic data to test the applicability of the existing models in detail.

II. EXPERIMENTAL RESULTS

This work was performed at the Indiana University Cyclotron Facility utilizing 80, 100, 136, and 164 MeV proton beams in the low-intensity target area, especially designed for in-beam γ-ray measurements. Beam intensity on the target was typically 0.5 nA. The transmitted beam was collected in a well shielded Faraday cup for current integration. Gamma rays produced produced by the proton bombardment of isotopically enriched[58-64]Ni targets (about 1 mg/cm^2 in thickness) were detected by a lithium-drifted germanium Ge(Li) crystal which had an efficiency of 10% compared to a 7.6 cm$\times$7.6 cm NaI detector for the 1332 keV line of a ^{60}Co source placed at 25 cm. Most measurements were made with the Ge(Li) at 90°, 3 to 5 cm from the target, with varying thicknesses of lucite absorber placed between the detector and target to protect against charged particle damage to the crystal. Some measurements were made at 125° to determine anisotropy corrections to the γ-ray cross sections, for which the detector was moved back to 12 cm. For each geometry during every run an efficiency and energy calibration of the Ge(Li) detector was made by using a mixed radioactive source in the target position. The mixed source consisted of known amounts of ^{109}Cd, ^{57}Co, ^{139}Ce, ^{113}Sn, ^{137}Cs, ^{60}Co, and ^{88}Y giving calibration points over an energy range of 88 to 1836 keV.

Overall γ-ray energy resolution varied from 2.5 to 3.0 keV full width at half maximum (FWHM) during the course of the measurements. The time of production of γ rays relative to the incident beam burst (about 1 nsec wide) was also determined using convéntional electronics techniques. Efforts were made to optimize the timing resolution over a large energy range and an FWHM of 5 nsec for the prompt peak in the time spectrum for higher energy γ rays (>800 keV) was typically obtained. Nevertheless, the timing resolution for lower energy γ rays grew progressively worse and was comparable to the time between the beam bursts (30 nsec) for γ rays lower than 200 keV in energy, which limited the usefulness of the timing information.

The dead time of the electronics and the data acquisition system was determined by feeding a pulser, triggered by the current integrator, into the preamplifier of the Ge(Li) detector and by comparing the number of pulser triggers to the total number of counts in the pulser peak in the Ge(Li) spectrum. Dead times averaged about 15%.

The linear energy and timing signals were digitized and routed to a computer for sorting and storage. Using software conditions three 4096 channel arrays for the prompt, delayed, and singles spectra and a 256 channel time spectrum were prepared. Each energy spectrum contained more than one hundred identifiable peaks which were fitted to Gaussian shapes by a computer program to extract peak areas. The latter were used to determine the production cross sections for each gamma ray after normalizing for the incident number of protons, the target thickness, the detection efficiency, and the dead time. Typically, adequate statistics were obtained to observe gamma rays produced with cross sections as low as 2 mb with an accuracy of about 10%. However, major uncertainty in the measured cross section was introduced by the unstripping of two or more overlapping peaks, especially when it involved one or more weak peaks. Whenever possible, contribution to the peaks in the prompt spectrum due to the decay process was determined using the corresponding delayed spectrum. However, as mentioned above, the in-beam timing information was often not adequate to allow an accurate determination of the delayed component for lower energy γ rays. For these recourse had to be made to off-line activation measurements which will be described elsewhere.[2]

Systematic uncertainties associated with the absolute cross sections due to charge integration,

TABLE I. Assignments, energies, and production cross section (and the associated percent errors) of the gamma rays observed in 164 MeV proton bombardment of ^{62}Ni.

Nucleus γ ray assigned	Gamma energy (fitted) keV	Production cross sections mb	Error in cross sections %
^{56}Mn	104.0	1.5	68
BKD (^{19}F)	110.1	7.3	13
^{58}Co	112.1	4.5	20
^{57}Fe	122.0	35.8	3
^{55}Mn	125.8	11.1	8
^{57}Fe	136.5	5.8	15
^{54}Fe	146.0	0.8	107
^{54}Mn	156.1	13.3	7
^{56}Co, ^{60}Co	158.4	8.9	10
BKG (^{19}F)	198.0	39.9	3
^{54}Mn, ^{48}V, ^{56}Mn	211.8	10.3	6
^{50}V	226.6	2.6	24
^{60}Co	229.7	4.2	16
^{51}Mn	238.3	3.6	19
^{54}Mn	252.8	2.3	36
^{60}Co	254.3	0.6	124
^{55}Fe, ^{56}Mn	273.6	5.7	12
^{60}Co	277.1	2.6	27
^{61}Ni	282.9	4.0	16
BKD?	295.6	3.3	24
^{48}V, ^{55}Mn	309.1	0.6	141
^{51}Cr, ^{56}Mn	315.6	2.4	33
^{51}V	320.1	5.1	17
^{58}Co	320.8	7.9	12
^{61}Co	333.5	4.9	20
^{59}Ni	339.4	18.5	5
BKD (^{21}Ne)	350.7	10.8	9
^{57}Fe	352.3	5.1	16
^{58}Co	365.6	5.0	14
^{53}Mn	376.8	3.5	22
^{55}Fe	384.8	1.5	50
^{60}Co	389.8	4.5	15
^{54}Fe, ^{55}Fe	411.7	6.5	12
BKD (^{26}Al)	416.9	15.7	4
^{48}V	427.8	1.0	62
^{58}Co, ^{50}Mn	432.9	4.7	16
^{60}Co	436.5	2.4	30
BKD (^{23}Na)	439.9	17.7	4
^{60}Co, ^{52}Mn	448.0	0.6	121
^{57}Co, ^{59}Ni	466.1	5.3	23
^{60}Ni	467.0	4.1	25
BKD (^{24}Ne)	472.2	9.1	13
^{55}Fe, ^{59}Fe	477.3	10.0	13
^{60}Co	482.3	3.9	33
^{60}Cu, ^{60}Ni	493.4	1.3	76
annihilation	511.0	318.5	1
^{60}Co	555.8	1.0	88
^{57}Fe	571.1	0.5	173
^{56}Co, ^{59}Co	575.7	3.6	27
BKD (^{22}Na)	584.2	20.3	6
^{55}Fe	605.0	11.6	9
^{51}V?	609.4	14.5	8
^{48}V	627.4	0.8	144
^{50}Mn?	648.9	0.5	170
^{61}Ni	656.0	1.1	92
^{50}Cr, BKD	661.8	22.0	5
^{54}Mn	704.7	3.8	27

TABLE I. (*Continued.*)

Nucleus γ ray assigned	Gamma energy (fitted) keV	Production cross sections mb	Error in corss sections %
^{58}Co, ^{60}Co, ^{53}Mn	727.6	1.6	72
^{52}Mn	731.0	0.6	177
^{52}Cr	744.3	13.1	8
^{51}Cr	749.7	4.8	22
^{50}Cr	782.6	2.6	44
^{60}Co	785.9	3.2	35
^{55}Fe	803.9	0.8	140
^{51}Cr	808.1	0.8	120
^{58}Fe	811.3	6.7	16
^{56}Co	811.4	8.7	12
^{60}Ni	826.4	12.8	10
^{56}Co, BKD (^{26}Al)	830.1	10.7	11
^{54}Cr	834.9	20.3	6
^{54}Mn, ^{50}V	839.6	8.0	16
BKD (^{27}Al)	843.9	44.6	3
^{56}Fe, ^{55}Fe, ^{52}Cr	846.9	146.5	1
^{54}Mn?, ^{57}Mn?	851.6	2.7	39
^{55}Mn	858.4	2.7	42
^{58}Fe	864.3	0.9	121
^{52}Mn	869.3	10.6	12
^{59}Ni	879.0	1.7	70
^{50}Mn, ^{46}Ti, ^{51}Ti	890.7	3.8	28
^{57}Fe	898.4	0.6	174
^{61}Ni	909.5	5.3	25
^{53}Mn	913.2	3.6	36
^{55}Fe	931.3	8.2	14
^{52}Cr	935.2	12.4	9
^{54}Co, ^{49}Cr	937.0	9.3	13
^{61}Ni	947.8	8.0	17
^{61}Cu	970.7	0.6	206
^{45}Sc?	974.7	7.0	18
^{48}Ti	983.8	13.3	10
^{54}Mn, ^{57}Mn?	991.5	4.6	34
^{59}Ni	998.5	2.4	61
^{58}Ni	1004.2	7.4	21
^{53}Cr	1006.6	5.1	27
^{56}Co	1010.5	6.7	20
BKD (^{27}Al)	1014.5	69.6	3
^{60}Ni, ^{61}Co, ^{54}Fe	1027.5	1.0	130
^{56}Fe	1038.1	14.6	10
^{58}Co	1044.4	2.0	72
^{58}Co	1051.1	6.4	24
^{57}Mn?	1062.1	5.9	26
^{59}Co, ^{50}Cr	1099.4	9.6	17
^{58}Cu?	1106.9	3.2	38
^{56}Co	1114.4	2.6	51
^{62}Ni	1129.9	6.4	24
^{54}Fe	1130.2	7.4	20
^{62}Ni	1162.4	3.9	27
^{51}Cr	1165.6	9.2	13
^{62}Ni, ^{60}Ni	1173.3	30.9	4
^{61}Ni	1185.7	2.2	54
^{59}Ni, ^{59}Co	1190.4	9.3	15
^{61}Co	1205.3	3.3	54
^{55}Fe	1223.2	10.4	21
^{57}Co	1223.7	7.2	30
^{56}Fe, ^{58}Co	1238.4	84.5	2
^{58}Fe	1265.7	2.4	57

TABLE I. (*Continued.*)

Nucleus γ ray assigned	Gamma energy (fitted) keV	Production cross sections mb	Error in cross sections %
BKD (^{22}Na)	1274.7	33.2	4
^{59}Co	1291.7	1.1	154
^{60}Ni	1293.8	3.5	41
^{56}Fe	1303.8	6.0	23
^{56}Fe, ^{48}Ti	1312.2	13.7	12
^{55}Fe	1316.6	8.4	18
^{60}Ni, ^{52}Cr	1332.8	50.0	4
^{59}Ni	1337.9	1.5	99
BKD (^{24}Mg)	1368.8	101.5	2
^{57}Co	1378.2	6.0	31
^{54}Fe, ^{55}Fe	1408.5	11.2	12
^{59}Ni	1428.7	7.4	19
^{52}Cr	1434.3	27.4	5
^{53}Mn	1441.1	9.2	15
^{54}Co?	1446.8	0.7	163
^{58}Ni	1454.3	13.8	11
BKD (^{40}K), ^{61}Ni	1460.7	32.2	4
^{59}Co	1462.3	1.9	83
^{51}Cr	1481.0	2.1	71
^{59}Co	1481.4	3.2	51
^{55}Mn	1529.0	6.6	26
^{61}Ni	1543.0	0.6	270
^{50}Ti	1553.2	1.4	123
^{61}Ni?	1610.5	8.6	20
^{54}Co	1614.1	1.4	95
BKD, ^{52}Cr?	1633.5	28.7	8
BKD	1731.3	4.8	30
^{57}Co, ^{60}Ni	1756.9	0.7	175
^{59}Ni?	1778.9	12.2	13
^{59}Ni?	1800.5	9.1	24
^{59}Ni	1801.4	0.7	344
BKD (^{26}Mg)	1808.7	84.6	4
^{57}Co	1898.1	3.8	67

dead time corrections, target thickness, and detection efficiency are estimated to be about 15%. The corresponding uncertainty for the 80 MeV measurements for ^{58}Ni and ^{62}Ni and 100 MeV measurements with a ^{64}Ni target is estimated to be 30% because of a bias in charge integration due to an alternating current pick up in the Faraday cup for the first case and because of poor integration at low currents ($\leq$0.1 nA) employed in the second case. Relative uncertainties in the cross sections vary widely and depend not only on the statistics but often on the accuracy with which overlapping peaks could be separated and, in a number of cases, on the precision with which the delayed components could be subtracted.

Observed gamma rays were assigned to a particular final nucleus on the basis of the measured energies and the consistency of relative intensity patterns with those expected for γ-ray transitions belonging to one or more cascades for that nucleus. For this purpose a list of gamma rays assigned on the basis of in-beam measurements to nuclei with $44 \leq A \leq 65$ and their relative location in their decay schemes was prepared from the recently published literature. In Table I are listed the energies, the production cross sections (including the percent uncertainties), and the assignment to possible final nucleus (or nuclei) for each gamma ray observed in the 164 MeV proton bombardment of ^{62}Ni. The contribution of a given gamma ray to each of the many final nuclei, wherever applicable, was determined using the observed intensities of other gamma rays belonging to the same cascade and the branching ratios published in the literature. The details and reservations pertaining to individual assignments can be found elsewhere.[12]

Cross sections for the production of individual final nuclei were obtained by summing observed cross sections for gamma rays assigned to transition to the ground state and to the known isomeric

TABLE II. Production cross sections for various final nuclei from in-beam γ-ray measurements with 80, 100, 136, and 164 MeV proton bombardment of ^{58}Ni target.

Final nucleus	Production cross sections (mb) 80 MeV	100 MeV	136 MeV	164 MeV
^{58}Ni	31 ± 3	29 ± 3	17 ± 2	9 ± 2
^{57}Ni	33 ± 3	34 ± 5	31 ± 5	23 ± 9
^{57}Co	38 ± 10	35 ± 10	32 ± 10	21 ± 8
^{56}Co	70 ± 15	74 ± 15	53 ± 8	43 ± 7
^{55}Co	4 ± 2	2 ± 2	2 ± 2	2 ± 2
^{54}Co	<2	<2	<2	<2
^{56}Fe	28 ± 5	27 ± 5	25 ± 5	20 ± 8
^{55}Fe	77 ± 14	70 ± 13	53 ± 10	42 ± 8
^{54}Fe	53 ± 5	60 ± 6	47 ± 5	30 ± 4
^{53}Fe	6 ± 3	10 ± 3	8 ± 3	6 ± 2
^{52}Fe	2 ± 2	2 ± 2	2 ± 2	<3
^{55}Mn	2 ± 2	3 ± 2	2 ± 2	3 ± 2
^{54}Mn	19 ± 4	13 ± 3	14 ± 3	9 ± 3
^{53}Mn	27 ± 5	38 ± 6	34 ± 6	30 ± 6
^{52}Mn	9 ± 4	10 ± 4	14 ± 4	11 ± 4
^{51}Mn	12 ± 2	11 ± 2	10 ± 2	8 ± 2
^{54}Cr	1 ± 1	2 ± 2	4 ± 2	5 ± 3
^{53}Cr	2 ± 2	4 ± 3	7 ± 3	3 ± 3
^{52}Cr	12 ± 2	14 ± 2	19 ± 4	20 ± 6
^{51}Cr	16 ± 3	14 ± 3	13 ± 3	11 ± 3
^{50}Cr	9 ± 2	21 ± 2	23 ± 2	18 ± 4
^{49}Cr	2 ± 1	3 ± 2	5 ± 2	6 ± 2
^{48}Cr	1 ± 1	1 ± 1	1 ± 1	1 ± 1
^{50}V	2 ± 1	3 ± 2	4 ± 2	3 ± 2
^{49}V	6 ± 4	10 ± 4	17 ± 5	17 ± 5
^{48}V	4 ± 2	4 ± 2	7 ± 3	7 ± 3
^{47}V	1 ± 1	2 ± 2	3 ± 2	4 ± 2
^{50}Ti	<2	<2	<2	<2
^{49}Ti	<2	<2	<2	<2
^{48}Ti	2 ± 1	3 ± 2	6 ± 2	6 ± 4
^{46}Ti	1 ± 1	3 ± 2	5 ± 2	8 ± 2

TABLE III. Production cross section for various final nuclei from in-beam γ-ray measurements with 100 and 136 MeV proton bombardment of ^{60}Ni.

Final nucleus	Production cross section (mb) 100 MeV	136 MeV
^{60}Ni	42 ± 4	25 ± 3
^{59}Ni	89 ± 10	63 ± 8
^{58}Ni	39 ± 4	28 ± 3
^{57}Ni	8 ± 5	7 ± 5
^{59}Co	16 ± 6	12 ± 6
^{58}Co	49 ± 7	47 ± 7
^{57}Co	63 ± 10	43 ± 8
^{56}Co	27 ± 6	18 ± 5
^{55}Co	2 ± 2	2 ± 2
^{58}Fe	4 ± 2	1 ± 1
^{57}Fe	12 ± 3	18 ± 4
^{56}Fe	62 ± 8	53 ± 7
^{55}Fe	60 ± 8	45 ± 8
^{54}Fe	17 ± 4	22 ± 4
^{53}Fe	1 ± 1	5 ± 2
^{56}Mn	4 ± 3	3 ± 3
^{55}Mn	16 ± 3	12 ± 3
^{54}Mn	21 ± 3	26 ± 4
^{53}Mn	15 ± 3	19 ± 3
^{52}Mn	8 ± 6	8 ± 6
^{51}Mn	3 ± 2	3 ± 2
^{54}Cr	6 ± 4	8 ± 4
^{53}Cr	10 ± 8	14 ± 10
^{52}Cr	11 ± 3	12 ± 3
^{51}Cr	4 ± 2	11 ± 3
^{50}Cr	3 ± 2	9 ± 2
^{49}Cr	2 ± 2	3 ± 2
^{50}V	3 ± 2	4 ± 2
^{49}V	4 ± 3	8 ± 3
^{48}V	4 ± 3	5 ± 3
^{50}Ti	<2	<2
^{49}Ti	<2	<2
^{48}Ti	1 ± 1	5 ± 2
^{46}Ti	1 ± 1	1 ± 1

states of the respective nucleus. The measured in-beam cross sections for the ^{58}Ni, ^{60}Ni, and ^{64}Ni targets for different proton energies are given in Tables II to V, respectively. It should be noted that the in-beam measurements yield only a lower limit for the production cross sections for a given nucleus since weak transitions to and direct production of the ground state are not observed. This effect is expected to be particularly large for odd A and odd-odd nuclei and indeed the activation measurements often yield considerably greater cross sections for these cases than the in-beam studies. For even-even nuclei this should be a small correction since the decay is mostly funneled through the first 2^+ state.

III. MODEL CALCULATIONS

Comparisons were made between measured cross sections and those predicted by hybrid[13] and cascade models.[14-16] Both models calculate nucleon emission from the nonequilibrated nuclear system of the incident proton plus the target nucleus, the so-called pre-equilibrium phase. Once equilibrium is attained, statistical techniques are employed to determine the evaporation of nucleons and clusters such as deuterons and alpha particles. Cross sections for the production of final nuclei as the end product of both kinds of emissions are calculated and correspond to the cross sections of specific nuclei measured in this study.

The hybrid model operates in phase space and describes the change of state of the nucleus, as it proceeds toward equilibrium, by a change in the number of excitons (excited particles and holes). The cascade model follows the trajectories of the incident and struck particles in real, or geometric, space. The hybrid model follows the evolvement of the reaction until the number of excitons reaches its equilibrium value. The cascade model

TABLE IV. Production cross section for various final nuclei from in-beam γ-ray measurements with 80, 100, 136, and 164 MeV proton bombardment of ^{62}Ni.

Final nucleus	Production cross sections (mb) 80 MeV	100 MeV	136 MeV	164 MeV
^{62}Ni	30 ± 10	30 ± 10	18 ± 10	11 ± 7
^{61}Ni	76 ± 20	54 ± 20	49 ± 15	48 ± 15
^{60}Ni	77 ± 7	74 ± 7	64 ± 7	52 ± 5
^{59}Ni	52 ± 6	47 ± 6	41 ± 6	31 ± 5
^{58}Ni	23 ± 3	18 ± 2	19 ± 2	14 ± 2
^{61}Co	3 ± 2	2 ± 2	6 ± 3	4 ± 3
^{60}Co	10 ± 4	13 ± 5	14 ± 5	13 ± 5
^{59}Co	17 ± 6	17 ± 6	17 ± 6	17 ± 6
^{58}Co	41 ± 7	37 ± 7	39 ± 7	35 ± 8
^{57}Co	21 ± 5	27 ± 6	24 ± 5	19 ± 6
^{56}Co	3 ± 2	6 ± 3	7 ± 3	8 ± 4
^{58}Fe	6 ± 2	6 ± 2	9 ± 2	9 ± 4
^{57}Fe	9 ± 2	13 ± 3	17 ± 3	17 ± 6
^{56}Fe	26 ± 5	36 ± 5	44 ± 5	52 ± 12
^{55}Fe	21 ± 5	21 ± 5	25 ± 5	24 ± 4
^{54}Fe	4 ± 2	7 ± 2	9 ± 2	8 ± 2
^{56}Mn	1 ± 1	2 ± 2	4 ± 3	5 ± 3
^{55}Mn	7 ± 2	11 ± 3	13 ± 3	18 ± 4
^{54}Mn	8 ± 2	18 ± 3	20 ± 4	21 ± 4
^{53}Mn	1 ± 1	4 ± 2	9 ± 4	13 ± 4
^{51}Mn	1 ± 1	2 ± 2	2 ± 2	4 ± 2
^{54}Cr	7 ± 4	8 ± 2	11 ± 2	12 ± 8
^{53}Cr	2 ± 2	2 ± 2	2 ± 2	5 ± 3
^{52}Cr	4 ± 2	5 ± 2	11 ± 3	13 ± 8
^{51}Cr	2 ± 2	2 ± 2	4 ± 3	12 ± 6
^{50}Cr	1 ± 1	1 ± 1	2 ± 2	3 ± 2
^{50}V	1 ± 1	1 ± 1	2 ± 2	3 ± 2
^{49}V	<2	<2	2 ± 2	2 ± 2
^{48}V	<2	<2	2 ± 2	2 ± 2
^{50}Ti	<2	<2	2 ± 2	2 ± 2
^{48}Ti	1 ± 1	3 ± 2	4 ± 2	6 ± 4
^{46}Ti	1 ± 1	2 ± 2	1 ± 1	4 ± 2

TABLE V. Production cross sections for various final nuclei from in-beam γ-ray measurements with 100 and 136 MeV proton bombardment of ^{64}Ni.

Final nuclei	Production cross sections (mb) 100 MeV	136 MeV
^{64}Ni	29 ± 4	14 ± 2
^{63}Ni	59 ± 10	50 ± 10
^{62}Ni	90 ± 12	69 ± 10
^{61}Ni	62 ± 20	45 ± 15
^{60}Ni	53 ± 6	41 ± 5
^{59}Ni	32 ± 5	27 ± 5
^{58}Ni	17 ± 2	17 ± 2
^{63}Co	10 [a]	10 [a]
^{62}Co	22 [a]	22 [a]
^{61}Co	11 ± 4	10 ± 4
^{60}Co	35 ± 10	22 ± 8
^{59}Co	13 ± 6	16 ± 6
^{58}Co	29 ± 7	41 ± 8
^{57}Co	11 ± 5	15 ± 5
^{56}Co	3 ± 3	3 ± 3
^{58}Fe	10 ± 2	13 ± 2
^{57}Fe	17 ± 6	29 ± 7
^{56}Fe	31 ± 5	38 ± 5
^{55}Fe	13 ± 4	10 ± 3
^{54}Fe	<2	<2
^{56}Mn	2 ± 2	7 ± 3
^{55}Mn	14 ± 4	19 ± 4
^{54}Mn	9 ± 6	17 ± 10
^{53}Mn	3 ± 2	10 ± 4
^{54}Cr	10 ± 3	11 ± 3
^{53}Cr	<2	<2
^{52}Cr	5 ± 2	5 ± 2
^{51}Cr	<4	<4

[a] These cross sections are estimated from systematics of activity measurements for other Ni targets.

assumes the nucleus to be at equilibrium when all the cascade particles that are not emitted fall below an arbitrary cutoff energy. The hybrid model calculates the emission probability of nucleons in a statistical manner and converges to the evaporation formalism for large numbers of excitons. For the cascade model, a nucleon reaching the nuclear surface is assumed to be emitted, although provision for reflection or refraction by the changing nuclear potential is sometimes included.

In spite of these different calculational philosophies, the models incorporate many of the same ideas on the reaction mechanism. Both divide the reaction into fast (pre-equilibrium) and slow (equilibrium) components. Both use free nucleon-nucleon scattering cross sections, corrected to account for the Pauli principle, to determine the transition rates (hybrid model) or collision rates (cascade model). The hybrid model has an option to determine this information using optical model parameters which fit elastic nucleon-nucleus scattering, but this option has not been used in the present analyses since knowledge of the optical potential in this energy range is only now being obtained.

The computer codes used for the hybrid model calculations are ALICE (Refs. 17, 18) and EVAHYB (Ref. 19) which were developed at the University of Rochester. Only the geometry-dependent-hybrid (GDH) option was used in ALICE. With this option (GDH) the code calculates the reaction for each partial wave separately, increasing the mean free paths for the larger partial waves which see more of the diffuse nuclear surface, and also modifies the particle-hole level densities. EVAHYB includes a provision for multiple pre-equilibrium emission but does not include the geometric effects.

The computer code used for the cascade calculations is VEGAS (Ref. 15) which incorporates a nonconstant nuclear density distribution and potential and provides an option to treat reflection or refraction at the potential boundaries. The subse-

quent evaporation computations were performed using two separate computer codes: (1) DFFMH (Ref. 20) which utilizes the Monte Carlo technique to calculate evaporation of particles using the Weisskopf evaporation formula, and (2) a modified[12] ALICE calculation which sorts the VEGAS results to determine the distribution of excitation energy after the cascade for each residual nucleus and calculates the Weisskopf evaporation in the same way that was done for the hybrid model. The DFFMH code is the one generally used with VEGAS, and the modified ALICE calculation allows direct comparison of the different pre-equilibrium calculations since the same evaporation calculation could be utilized. Also, since the two evaporation codes can be used with the same pre-equilibrium calculation (VEGAS), the effect due to different treatment of the evaporation in the two codes on the final results could be directly compared.

All computer codes were adapted to the Indiana University Cyclotron Facility's Harris 6024 computers, utilizing the virtual memory VULCAN operating system. There are several possible combinations of input parameters that can be used for ALICE, EVAHYB, VEGAS, and DFFMH. The ones used in this work are listed in the Appendix.

IV. DISCUSSION OF RESULTS

A. Absolute cross section

The total observed cross section obtained by summing the production cross sections of all final nuclei (see Tables II to V) for a given target and proton energy are listed in Table VI for various cases along with those including the radioactivity results[2] for a few cases. There appears to be some tendency for the summed cross sections to decrease with increasing bombarding energy, although this effect is barely discernable and may, at any rate, merely be the result of unassigned cross section due to increasing complexity of the gamma spectra as the bombarding energy is increased. The magnitudes of the cross section reported here for ^{58}Ni target are consistent with those reported in Ref. 11 but disagree by a large factor with those reported in Ref. 10.

For comparison total reaction cross sections predicted by the optical model calculation using the code ALICE and those given by the cascade model are also listed in Table VI. The cascade model computes the reaction cross section by multiplying the geometric cross section by the ratio of the number of incident protons which interact in the nucleus to the total number of trials. The observed in-beam cross sections are typically 50–70 % of the optical model reaction cross sections and 60–80 % of the cascade model values. With activation results the observed values become 65–75 % and 80–90 % of the two predicted values, respectively.

B. Cross section distributions

In Tables VII through IX are listed the predicted cross sections for individual final nuclei for the cases of 80 and 164 MeV protons on a ^{62}Ni target and for 164 MeV protons on a ^{58}Ni target, respectively, along with the corresponding observed values (including the activation results). For an overall graphic view, the experimental cross sections are plotted in Fig. 1 for a ^{62}Ni target at two energies and the values predicted by EVAHYB and VEGAS are plotted in Fig. 2 for the case of 164 MeV protons on ^{62}Ni. Features of the observed

TABLE VI. Total observed and calculated reaction cross sections.

Target nucleus	Proton energy (MeV)	Reaction cross sections (mb) Observed in-beam	Observed in-beam plus activity	Optical model	VEGAS	Geometric
^{58}Ni	80	463 [a]	637	845	678	1281
	100	495		804	674	1302
	136	452		786	659	1324
	164	361	531	763	647	1334
^{60}Ni	100	597		822	696	1321
	136	534		801	657	1343
^{62}Ni	80	629 [a]	772	884	717	1318
	100	465		840	710	1340
	136	481	611	816	691	1362
	164	477	606	800	683	1373
^{64}Ni	100	736 [a]		858	717	1358
	136	522		830	711	1381

[a] These cross sections are relatively more uncertain owing to reasons stated in the text.

TABLE VII. Comparison of the observed production cross sections for final nuclei with those predicted by various models for the case of 80 MeV proton bombardment of ^{62}Ni.

Final nuclei	Observed	Production cross sections (mb) GDH (MFP×1)	EVAYHB (MFP×2)	VEGAS + DFFMH	VEGAS + ALICE
^{62}Cu	20 ± 8 [a]	14	4	18	18
^{61}Cu	12.4 ± 0.6 [a]	12	3	26	14
^{60}Cu	5.2 ± 1 [a]	4	1	20	4
^{62}Ni	30 ± 10	23	9	29	22
^{61}Ni	76 ± 20	53	69	91	89
^{60}Ni	77 ± 7	74	102	66	77
^{59}Ni	52 ± 6	54	83	67	48
^{58}Ni	23 ± 3	27	45	69	20
^{57}Ni	2.3 ± 0.1 [a]	6	8	10	6
^{56}Ni	0.8 ± 0.3 [a]	0.1	0.07	0.1	0.08
^{61}Co	23 ± 2 [a]	2	4	14	17
^{60}Co	32 ± 3 [a]	10	16	22	23
^{59}Co	17 ± 6	31	48	29	37
^{58}Co	82 ± 4 [a]	86	100	46	75
^{57}Co	52 ± 3 [a]	69	77	59	64
^{56}Co	6 ± 1 [a]	15	12	23	18
^{55}Co	1.5 ± 0.1 [a]	5	3	4	3
^{59}Fe	2.3 ± 0.4 [a]	1	1	2	2
^{58}Fe	6 ± 2	7	6	6	7
^{57}Fe	9 ± 2	22	13	9	23
^{56}Fe	26 ± 5	29	21	26	23
^{55}Fe	21 ± 5	70	36	40	34
^{54}Fe	4 ± 2	21	25	7	22
^{53}Fe	<1 [a]	0.03	0.04	0.3	0.3
^{52}Fe	0.02 ± 0.005	0	0	<0.1	0
^{56}Mn	2.5 ± 0.2 [a]	2	1	1	2
^{55}Mn	7 ± 2	15	5	9	8
^{54}Mn	13.0 [a] ± 1 [a]	36	11	10	34
^{53}Mn	1 ± 1	5	6	2	9
^{52}Mn	1.5 ± 0.2 [a,b]	8	1	2	3
^{51}Mn	1 ± 1	0.3	0.05	0.1	0.6
^{54}Cr	7 ± 4	0.3	0.2	0.2	0.6
^{53}Cr	2 ± 2	2	0.4	1	0.9
^{52}Cr	4 ± 2	10	6	2	5
^{51}Cr	2.5 ± 0.3 [a]	4	4	1	7
^{50}Cr	1 ± 1	0.01	0.01	0.1	0.1
^{49}Cr	<0.04	0	c	0.1	0
^{48}Cr	<0.005	0	c	0.1	0
^{50}V	1 ± 1	0.2	0.06	0.1	0.2
^{48}V	0.1 ± 0.04 [a]	0.03	c	0.1	0.1
^{48}Ti	1 ± 1	0.02	0.02	0.1	0.001
^{47}Ti	1 ± 1	0	c	0.1	0.001

[a] Deduced from activation measurements, Ref. 2.
[b] Does not include isomeric state production.
[c] Outside dimensioned limits of program.

cross section, which the models are able to reproduce quite well, are: (a) nuclei farther from the target nucleus are produced with progressively smaller cross sections at a given bombarding energy, (b) at higher bombarding energies nuclei farther from the target are produced with relatively larger cross sections at the expense of those near the target mass, and (c) the production cross sections of nuclei of a given Z show a peaked distribution with centroids lying near the line of stability. The cascade model on the whole not only gives a rather satisfactory account of the absolute magnitude of the observed cross sections, but also of trends among isotopes of various nuclear species. EVAHYB systematically predicts more cross sections for Mn, Cr, and V isotopes than those either observed or predicted by the cascade model. This discrepancy along with the necessity to in-

TABLE VIII. Comparison of the observed production cross sections for final nuclei with those predicted by various models for the case of 164 MeV proton bombardment of ^{62}Ni.

Final nuclei	Production cross sections (mb) Observed	EVAHYB (MFP × 2)	VEGAS + DFFMH	VEGAS + ALICE
^{62}Cu	12 ± 6 [a]	2	11	9
^{61}Cu	5.4 ± 0.2 [a]	2	15	9
^{60}Cu	1.7 ± 0.2 [a]	0.4	10	3
^{62}Ni	11 ± 7	4	15	12
^{61}Ni	48 ± 15	44	78	78
^{60}Ni	52 ± 5	65	46	52
^{59}Ni	31 ± 5	51	36	29
^{58}Ni	14 ± 2	20	29	11
^{57}Ni	1.3 ± 0.3 [a]	5	7	3
^{56}Ni	<0.4 [a]	0.5	0.4	0.2
^{61}Co	26 ± 4 [a]	4	19	18
^{60}Co	35 ± 5 [a]	12	18	19
^{59}Co	17 ± 6	30	26	30
^{58}Co	58 ± 2 [a]	51	29	44
^{57}Co	42 ± 4 [a]	57	41	33
^{56}Co	11 ± 1 [a]	30	28	20
^{55}Co	1.5 ± 0.2 [a]	8	6	5
^{59}Fe	3.1 ± 0.3 [a]	0.9	3	2
^{58}Fe	9 ± 4	4	5	4
^{57}Fe	17 ± 6	15	11	15
^{56}Fe	52 ± 12	32	30	25
^{55}Fe	24 ± 4	47	42	36
^{54}Fe	8 ± 2	31	19	19
^{53}Fe	1.0 ± 0.4 [a]	2	9	4
^{52}Fe	0.09 ± 0.02 [a]	0.08	0.7	0.3
^{56}Mn	3.6 ± 0.2 [a]	2	2	2
^{55}Mn	18 ± 4	8	11	7
^{54}Mn	25 ± 2 [a]	17	28	26
^{53}Mn	13 ± 4	38	19	34
^{52}Mn	6.1 ± 0.7 [a]	10	18	19
^{51}Mn	4 ± 2	1	4	4
^{54}Cr	12 ± 8	0.6	2	0.9
^{53}Cr	5 ± 3	3	8	5
^{52}Cr	13 ± 8	30	9	14
^{51}Cr	14 ± 1 [a]	20	13	22
^{50}Cr	3 ± 2	4	6	12
^{49}Cr	0.6 ± 0.1 [a]	c	2	3
^{48}Cr	0.05 ± 0.01 [a]	c	0.06	0.2
^{50}Ti	2 ± 2	0.3	0.4	0.3
^{48}Ti	6 ± 4	1	1	3
^{46}Ti	4 ± 2	3	0.6	3
^{48}Sc	0.13 ± 0.02 [a]	c	0.07	0.1
^{46}Sc	1.0 ± 0.3 [a]	c	0.2	0.8
^{44}Sc	0.19 ± 0.03 [a,b]	c	0.06	c
^{43}K	0.042 ± 0.007	c	0.03	c

[a] Deduced from activation measurements.
[b] Does not include isomeric state production.
[c] Outside dimensional limits of program.

crease the mean free path (MFP) by a factor of 2 to get reasonable comparison with the observations is expected to be corrected when the geometry-dependent effects arising from the diffuseness of the nuclear surface are incorporated, as appears to be the case for GDH predictions at 80 MeV (Table VII). As is obvious from a brief perusal of Tables VII through IX, there are a number of large quantitative discrepancies between the observed and predicted values. Some of these arise because

TABLE IX. Comparison of the observed production cross sections for final nuclei with those predicted by various models for the case of 164 MeV proton bombardment of ^{58}Ni.

Final nuclei	Production cross sections (mb) Observed	EVAHYB (MFP × 2)	VEGAS + DFFMH	VEGAS + ALICE
^{58}Ni	9 ± 2	4	19	10
^{57}Ni	46 ± 3 [a]	36	70	57
^{56}Ni	5.0 ± 0.7 [a]	8	11	8
^{57}Co	56 ± 6 [a]	15	40	43
^{56}Co	60 ± 8 [a]	63	67	64
^{55}Co	21 ± 2 [a]	38	27	28
^{54}Co	<2	2	15	4
^{56}Fe	20 ± 8	5	8	8
^{55}Fe	42 ± 8	40	41	38
^{54}Fe	30 ± 4	75	39	47
^{53}Fe	6 ± 2	14	33	17
^{52}Fe	2.6 ± 0.3 [a]	2	8	3
^{55}Mn	3 ± 2	0.3	1	0.6
^{54}Mn	18 ± 2 [a]	6	13	16
^{53}Mn	30 ± 6	76	16	40
^{52}Mn	17 ± 4 [a,b]	39	42	38
^{51}Mn	8 ± 2	8	22	16
^{54}Cr	5 ± 3	0.01	0.1	0.04
^{53}Cr	3 ± 3	0.4	2	1
^{52}Cr	20 ± 6	41	3	9
^{51}Cr	47 ± 7 [a]	52	22	28
^{50}Cr	18 ± 4	23	25	31
^{49}Cr	8 ± 2 [a]	4	19	14
^{48}Cr	1.2 ± 0.2 [a]	0.4	3	2
^{50}V	3 ± 2	24	5	9
^{49}V	17 ± 5	22	7	17
^{48}V	12 ± 2 [a]	10	17	22
^{47}V	4 ± 2	2	6	8
^{50}Ti	<2	0.2	0.04	0.08
^{49}Ti	<2	2	0.7	0.8
^{48}Ti	6 ± 4	8	2	3
^{47}Ti		9	6	12
^{46}Ti	8 ± 2	4	5	13
^{46}Sc	1.2 ± 0.3 [a]	c	0.5	1
^{44}Sc	1.5 ± 0.3 [d]	c	2	5

[a] Obtained from activation measurements.

[b] Does not include the cross section with which isomeric state is populated.

[c] There is no prediction for these cases due to limited dimensions of the mass removal variables in the program.

[d] Does not include the cross section with which ground state is populated.

the observed cross sections are only part of the total production cross sections, but in other cases, especially where activation results are available and the predicted values are smaller than the observed, these differences must be real.

C. Mass and charge removal

The average number of nucleons removed from the initially formed target plus proton system is

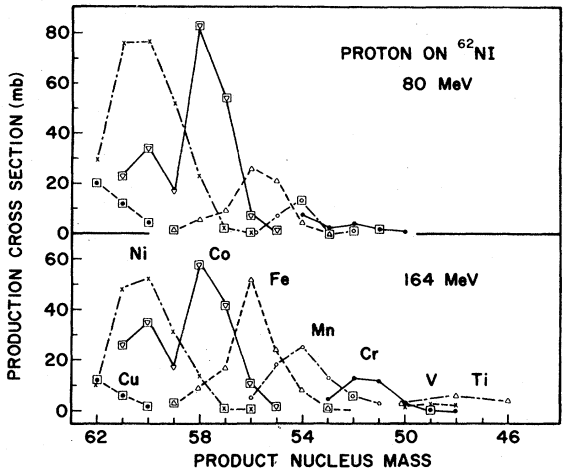

FIG. 1. Production cross sections of various final nuclei as a function of the product mass for the cases of 80 and 164 MeV proton bombardment of ^{62}Ni. Values of cross sections which are plotted with a rectangle surrounding the various symbols correspond to results obtained with activation technique.

defined to be

$$\langle \Delta A \rangle = \sum_i (\Delta A_i)\sigma_i / \sum_i \sigma_i , \qquad (1)$$

where ΔA_i is the difference in mass number of the ith final nucleus from that of the initial system and σ_i is the production cross section of the ith nucleus. Values of $\langle \Delta A \rangle$ based upon the observed cross sections are plotted (solid symbols) in the top portion of Fig. 3 and listed in Table X. A straight line trend of the observed values has a

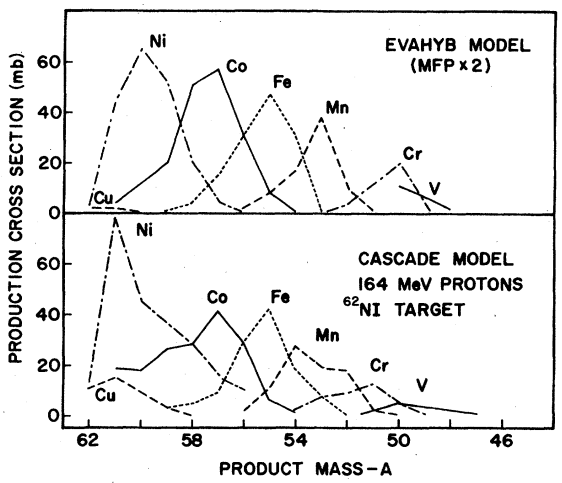

FIG. 2. Production cross sections of final nuclei as predicted by EVAHYB model using twice the mean free path given by the nucleon-nucleon cross sections (top section) and by the cascade model for the case of 164 MeV proton bombardment of ^{62}Ni (bottom section).

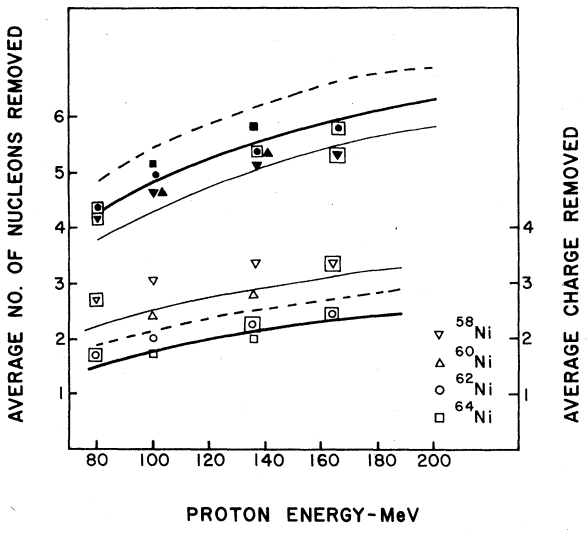

FIG. 3. Average number of nucleons removed $\langle \Delta A \rangle$ (solid symbols in top part) and protons removed $\langle \Delta Z \rangle$ (open symbols in lower part) from the target plus incident proton system as a function of the incident energy. The solid curves correspond to predictions by the cascade model for the cases of ^{58}Ni (thin line) and ^{62}Ni (thick line) targets. The dashed line corresponds to those of the hybrid model using the EVAHYB code and pertains to the ^{62}Ni target.

slope of 0.017 nucleons/MeV for the energy range of 80 to 164 MeV. This result immediately rules out total fusion of the incident proton with the target nucleus as a possible mechanism since this process would yield a slope of 0.1 nucleon/MeV. The single-emission hybrid model is similarly discarded because it predicts[12] a value of 0.05 nucleon/MeV. However, at 80 MeV the geometry-dependent-hybrid model (GDH) gives a value of $\langle \Delta A \rangle$ which is only half a nucleon higher than the observed value indicating that below this energy a single pre-equilibrium emission model may be adequate. In the energy range of 80 to 164 MeV the MFP×1 (see Appendix) calculation (not shown) with EVAHYB consistently predicts emission of about 1.5 nucleons more than is observed. This difference is about the same as that between the predictions of GDH and the simple hybrid model at 80 MeV. Therefore the MFP×2 (see Appendix) option which gives better overall agreement may be viewed as a means of simulating the geometry-dependent effects. Other than higher absolute values for $\langle \Delta A \rangle$ by about half a unit (dashed curve in Fig. 3), EVAHYB predicts $\langle \Delta A \rangle$ to increase with energy at the rate of 0.02 nucleon per MeV as does the cascade model (solid curves in Fig. 3) although the latter predicts the absolute magnitudes of $\langle \Delta A \rangle$ closer to those observed. Both models predict dependence of $\langle \Delta A \rangle$ on the isotopic nature of the targets which is somewhat less than that observed (see comparison for ^{58}Ni and ^{62}Ni cases in Fig. 3).

Points (open symbols) and the set of curves in Fig. 3 correspond to the average amount of charge removal $\langle \Delta Z \rangle$ as a function of bombarding energy. The relative ability of the two model calculations to account for the energy and isotopic (target) dependence of $\langle \Delta Z \rangle$ is a little better than that found for $\langle \Delta A \rangle$ (see Sec. IV D for further discussion on this point).

D. Mass and charge distribution

The total observed cross sections for production of nuclei of a certain mass A or charge Z are plotted in Figs. 4 through 8 for ^{62}Ni and ^{58}Ni targets along with the corresponding results of various model calculations. The models are able to give a

TABLE X. Average number of nucleons $\langle \Delta A \rangle$ and protons $\langle \Delta Z \rangle$ removed from the initial proton plus target system.

Target	Energy MeV	Experimental $\langle \Delta Z \rangle$	Experimental $\langle \Delta A \rangle$	EVAHYB (MFP×2) $\langle \Delta Z \rangle$	EVAHYB (MFP×2) $\langle \Delta A \rangle$	VEGAS + DFFMH $\langle \Delta Z \rangle$	VEGAS + DFFMH $\langle \Delta A \rangle$	VEGAS + ALICE $\langle \Delta Z \rangle$	VEGAS + ALICE $\langle \Delta A \rangle$
^{58}Ni	80	2.8[a]	4.2[a]	2.9[b]	4.6[b]	2.3	3.9	2.8	4.5
^{58}Ni	100	3.1	4.6	3.2	5.0	2.5	4.3	3.1	5.0
^{58}Ni	136	3.4	5.1	3.5	5.6	2.9	5.0	3.4	5.7
^{58}Ni	164	3.3[a]	5.2[a]	3.7	5.9	3.1	5.4	3.6	6.0
^{60}Ni	100	2.5	4.6	2.7	5.2	2.1	4.5	2.6	5.3
^{60}Ni	136	2.8	5.3	3.0	6.0	2.4	5.1	2.9	5.9
^{62}Ni	80	1.7[a]	4.3[a]	1.8	4.8	1.6	4.4	1.9	4.9
^{62}Ni	100	2.0	4.9	2.1	5.3	1.8	4.9	2.2	5.5
^{62}Ni	136	2.2[a]	5.3[a]	2.3	6.1	2.1	5.4	2.5	6.1
^{62}Ni	164	2.4[a]	5.7[a]	2.5	6.5	2.3	5.9	2.7	6.6
^{64}Ni	100	1.8	5.1	1.5	5.5	1.5	4.9	1.7	5.5
^{64}Ni	136	2.0	5.8	1.9	6.2	1.7	5.5	2.0	6.1

[a] These values were derived including the cross sections determined through activation measurements.

[b] GDH model predicts essentially the same values but EVAHYB (MFP×1) gives values of 3.5 and 5.6 for $\langle \Delta Z \rangle$ and $\langle \Delta A \rangle$, respectively, for the 80 MeV case.

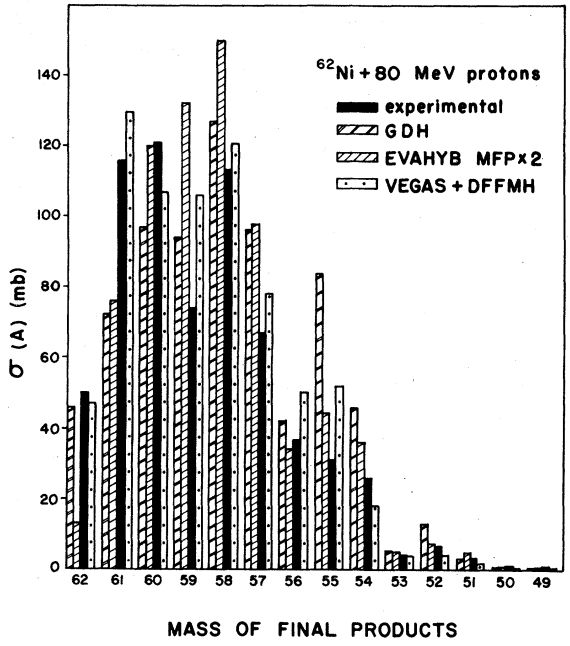

FIG. 4. Comparison of the observed cross sections (solid bars) for nuclei of various masses with those predicted by different models for 80 MeV proton bombardment of ^{62}Ni.

reasonable account of the trends in the observed distributions both with changes in the target mass and in the incident proton energy. GDH calculations seem to be in better agreement with observations at 80 MeV than those of EVAHYB, even with the MFP×2 option. EVAHYB systematically over-

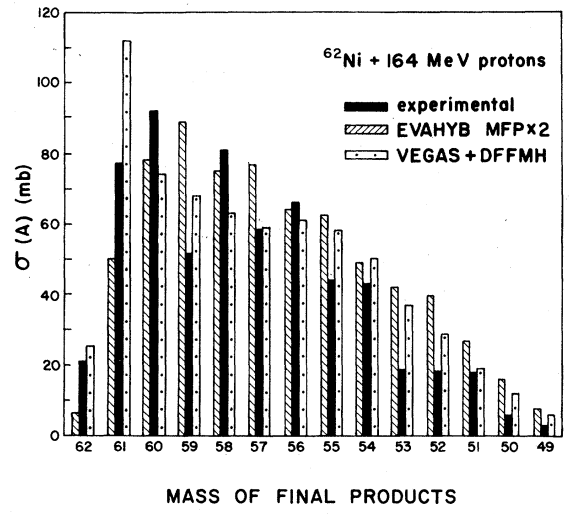

FIG. 5. Comparison of the observed cross sections (solid bars) for nuclei of various masses with those predicted by different models for 164 MeV proton bombardment of ^{58}Ni.

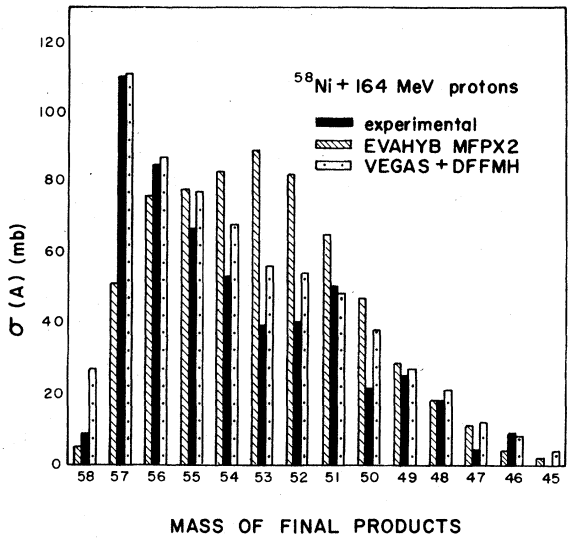

FIG. 6. Comparison of the observed cross sections (solid bars) for nuclei of various masses with those predicted by different models for 164 MeV proton bombardment of ^{62}Ni.

estimates the cross sections for lighter nuclei far from the target and underestimates for the heavier ones. VEGAS plus DFFMH gives, on the whole, a better account of the observed trends with A and Z

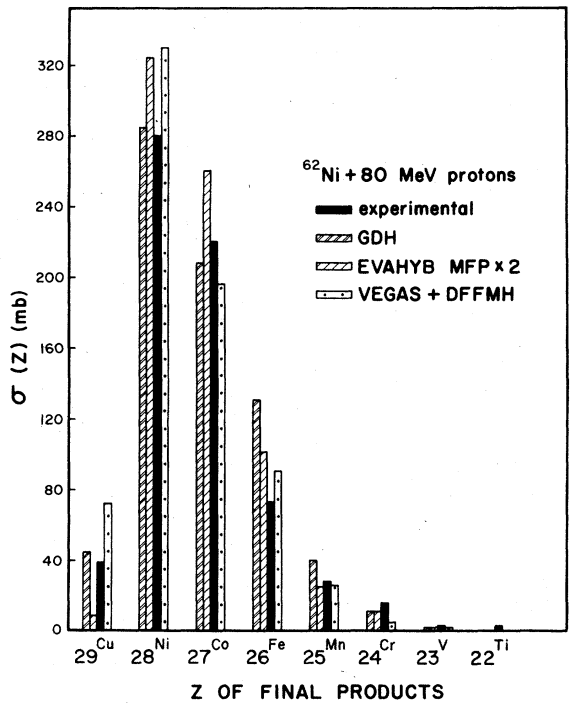

FIG. 7. Comparison of the observed cross sections (solid bars) for various nuclear species with those predicted by different models for 80 MeV proton bombardment of ^{62}Ni.

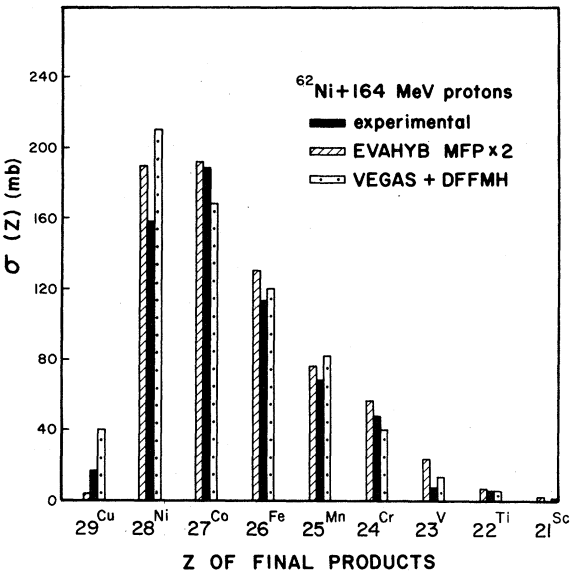

FIG. 8. Comparison of the observed cross sections (solid bars) for various nuclear species with those predicted by different models for 164 MeV proton bombardment of ^{64}Ni.

over the entire energy range for all targets, although it disagrees with the measurements for a number of product nuclei. Model predictions pertaining to the charge distributions are found to be more strongly dependent on the parameter values used in the evaporation phase of the calculation than do the mass distributions. To investigate this effect, evaporation calculations in conjuction with the output of VEGAS were performed using both DFFMH and the evaporation part of ALICE. A compliation of the average charge and mass removal for the two cases is given in Table X along with experimental values. ALICE systematically predicts about 0.6 more nucleon removed, although it reproduces the charge removed to within 0.1 unit (see Table X). On the other hand DFFMH tends to underpredict the charge removal by about 0.3 units and overpredicts the neutron removal by about the same amount, thus giving the average number of nucleons removed closer to those actually observed (see Fig. 3 and Table X). Since both codes are based upon the Weisskopf formulation[21] this difference ostensibly arises from details of how the inverse cross sections and level densities are calculated in the two codes. Since the same amount of excitation energy is dissipated through nucleon evaporation in both calculations, it implies that the average emission energies are less in ALICE than in DFFMH. Indeed for the case of 136 MeV protons on ^{58}Ni the average evaporation energies are 5.0, 8.9, 11.3, and 16.1 MeV in DFFMH for neutrons, protons, deuterons, and alpha particles,

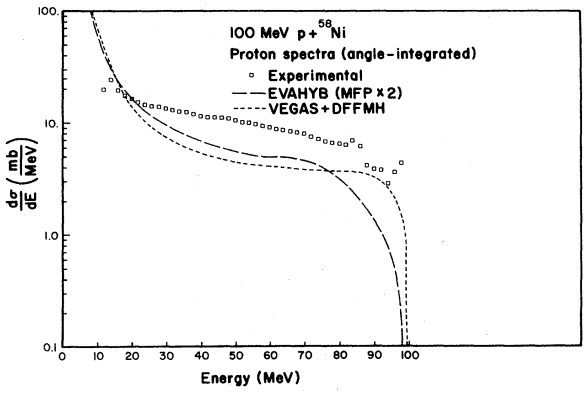

FIG. 9. Angle integrated proton energy spectrum observed (open squares) and those predicted by EVAHYB (dashed curve) and VEGAS (dotted curve) for the case of 100 MeV protons on ^{58}Ni. The experimental values were taken from Ref. 23.

respectively, whereas the corresponding values in ALICE are 3.5, 7.0, 9.6, and 13.9 MeV. It is obvious that there is still much to be learned about evaporation from highly excited nuclei and that existing uncertainties significantly affect the conclusions that can be drawn from the observations.

E. Energy and angular distribution of emitted protons

In Fig. 9 the observed angle integrated energy spectrum of protons following bombardment by 100 MeV protons on ^{58}Ni reported by Wu *et al.*[21] is reproduced along with corresponding predictions of EVAHYB (MFP × 2) and VEGAS plus DFFMH. Between 20 to 100 MeV there seems to be a discrepancy between the observed and the predicted cross sections, the latter being systematically lower than the former. VEGAS reproduces the shape of the

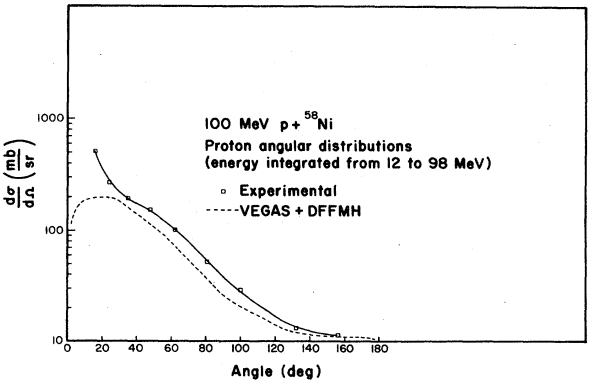

FIG. 10. Energy integrated angular distribution of protons emitted following 100 MeV proton bombardment of ^{58}Ni; solid curve is drawn through experimental points and dotted curve represents the predictions of the cascade model.

spectrum at higher energy noticeably better (not including the elastic peak) than EVAHYB. The discrepancies in shape and magnitude of the cross section for the lower (<20 MeV) end of the spectrum not being well determined because of experimental cutoffs or to inadequacies of the calculation in the equilibrium (or near-equilibrium) phase. In Fig. 10 the observed energy integrated (from 12 to 98 MeV) angular distribution of the emitted protons is compared with the predictions of VEGAS. Except at very forward angles where VEGAS predicts a peak and the observed distributions continue to rise, the calculations agree rather well with the observations in shape but are systematically lower in magnitude.

V. SUMMARY AND CONCLUSIONS

The measurements reported in this study pertain to the determination of the cross sections with which various final nuclei are produced following the bombardment of nickel isotopes by 80–164 MeV protons. The motivation was to provide a systematic set of experimental results to (a) gain insight about the characteristics of nucleon-nucleus interactions at intermediate energies, (b) test various existing models, and (c) compare results from proton-induced reactions with those for other projectiles. In particular, the earlier measurements[5-11] had highlighted the following results: (a) Nuclei which are an integral number of alpha particles removed from the target nucleus were produced with relatively larger cross section, and (b) the average number of nucleons removed from the target by pions did not vary over an incident pion energy range of 0 to 200 MeV. The first result had strong implications concerning the extent to which correlated clusters of nucleons either exist in nuclei or are dynamically formed in the course of an interaction. The second result begged for similar proton data at intermediate energy, with the hope that comparison of the results would point out similarities and differences in the reaction mechanism of these two types of projectiles. Other relevant questions regarding the reaction mechanism of medium energy nucleons with nuclei are: (a) In the pre-equilibrium phase, what are the relative roles of direct knockout, inelastic scattering, charge exchange and intranuclear cascade processes? (b) How many interactions or emissions take place in the pre-equilibrium (or fast) phase prior to attainment of equilibrium? (c) How is the incident energy shared between the fast emissions and the residual energy of the equilibrated system? (d) What are the relative roles of emission of different types of particles (p, n, d, t, ^{3}He, α, etc.) in the pre-equilibrium and evaporation phases? (e) How does the interaction vary with bombarding energy? (f) How are the measured quantities affected by the characteristics of the target nucleus, e.g., its neutron excess ($N-Z$)? (g) In what respects do the current models need to be extended to better account for the experimental results? (h) Are any physical quantities determined as a result of the comparisons with models?

The nucleon-nucleus interaction is envisaged as first proceeding through a pre-equilibrium phase in which the incident nucleon scatters off the target nucleons with the struck nucleon and the incident nucleon undergoing further scatterings or escaping from the nucleus. At the end of this phase the residual nucleus deexcites through the evaporation process. From the present data an estimate of the number of nucleons emitted in the pre-equilibrium phase can be made. The situation is most transparent in the case of ^{64}Ni as here a large fraction of the observed cross section, ~48% at 100 MeV and 50% at 136 MeV, goes into producing lighter nickel isotopes. Therefore, about half of the time only one proton is able to escape from the ^{64}Ni plus incident proton system during the pre-equilibrium phase. Noting that neutrons and protons should behave similarly in the pre-equilibrium phase, emission of one fast neutron is also quite likely. Thus, for ^{64}Ni in ~50% of the cases only one or two fast nucleons appear to be emitted, leaving the residual nuclei of ^{64}Cu, ^{64}Ni, and ^{63}Ni in a broad range of excitation from which the evaporation subsequently drives the production towards the lighter nickel isotopes lying near the line of stability. The rapid convergence toward the line of stability observed for all cases indicates that the number of pre-equilibrium nucleons emitted is of the same order for all targets. This constitutes the first time[1] that such a conclusion has been explicitly drawn from experimentally determined quantities and is one of the major results of this study.

The increase in $\langle \Delta A \rangle$ of 1 to 1.4 mass units from 80 to 164 MeV bombarding energy (see Fig. 4) shows that almost all the additional energy above 80 MeV is dissipated in the pre-equilibrium phase of the reaction. In the evaporation phase only about 10 MeV is needed for the emission of an additional nucleon. If all of the increase in $\langle \Delta A \rangle$ in going from 80 to 164 MeV were due to extra nucleons emitted in the evaporation phase, one would conclude that the average excitation energy of the residual equilibrated nuclei increased by 10–15 MeV. This number is an upper limit in the absence, as yet, of a direct measurement of the increase in the average energy of the particles in the fast phase. However, in terms of model calculations it appears that the pre-equilibrium emissions

are responsible for about half of this increase, i.e., the average number of pre-equilibrium particles emitted at 164 MeV is about 0.7 more than those at 80 MeV. Thus, it is likely that the average excitation energy of the equilibrated nuclei increases less than 10 MeV for the above mentioned range of incident energies. Given the fact that at 164 MeV the total $\langle \Delta A \rangle$ is about 5.5 and of this about two nucleons are emitted in the fast phase; then about 3.5 nucleons are emitted in the evaporation phase. This number corresponds to an average excitation of the system in equilibrium of about 45 MeV (the residual nucleus after evaporation may have about 10 MeV excitation energy). Thus, on an average about $\frac{2}{3}$ of the incident energy is taken away by pre-equilibrium emissions at 164 MeV. Similar arguments lead to the result that this fraction decreases to about $\frac{1}{2}$ at 80 MeV, which, in turn, confirms that (a) the average excitation energy following the pre-equilibrium phase does not increase rapidly with bombarding energy, and (b) its magnitude is about 40–45 MeV for the proton energy range of 80–164 MeV. However, the fact that one observes production of nuclei as much as 14 (10) mass units removed from the target mass with proton bombarding energy of 164 (80) MeV implies that the range of nuclear excitation over which nuclei are left after the pre-equilibrium emissions is rather broad, extending to within 10 MeV of the bombarding energy.

Relatively large cross sections with which "1α" ($2n$, $2p$) removed nuclei are produced with ^{58}Ni and ^{60}Ni targets (12% and 11% of the total observed cross section, respectively) are believed to be a consequence of the fact that for these targets the 1α nuclei lie close to the line of stability where the cross sections for nuclei of a given Z are observed to peak, in general. In contrast, for ^{62}Ni and ^{64}Ni the 1α removed nuclei lie relatively far from the line of stability and therefore the production cross sections for these nuclei are small. Since the nucleon removal through evaporation tends to drive the system toward the line of stability, the above results are not surprising and there is no reason, as yet, to postulate enhanced alpha removal for these reactions.

Extensive comparisons of experimental results with the cascade and hybrid models have been made in this work. Overall, the cascade model (VEGAS) exhibits better agreement with the observed results. Inclusion of surface effects in the multiple pre-equilibrium emission version of the hybrid model (EVAHYB) is shown to be necessary in order to obtain an equivalent accounting of the experimental cross sections. While there are significant differences between calculated and observed production cross sections, the overall capability of the models to predict the observed cross sections for the different targets and energy range covered here is convincing evidence that the dominant features of the mechanism for these reactions are incorporated in the calculations. In particular, the fact that calculated range in mass of products nuclei and the associated cross sections agree with those observed (see Figs. 4–6) implies that the models, especially VEGAS, are predicting the range of nuclear excitations (and the corresponding cross sections) left after the pre-equilibrium emissions essentially correctly. A sizeable discrepancy in this respect would have led to either under- or overprediction in the range of masses of the product nuclei.

Emission of high energy clusters (e.g., d, t, ^{3}He, and α) in the pre-equilibrium phase is not included in the hybrid and cascade models but is observed[4,22] with proton bombardment. Also, interactions which excite collective modes of various multipoles in the target nucleus through inelastic scattering are not included. However, there are indications that contributions from such processes may be significant; for example, the sharp rise in the angular distribution of the emitted protons in the forward direction in contrast to the predictions of the cascade model which predicts a peak at about 20° (Fig. 10).

A study of the model calculations (see Ref. 12 for details) reveal a few interesting results worthy of brief notice here. (1) Of a total of about five nucleons that are emitted on an average from various nickel targets, e.g., at 136 MeV, the models predict (see Fig. 11) that about two are emitted in the pre-equilibrium phase and the remaining three are

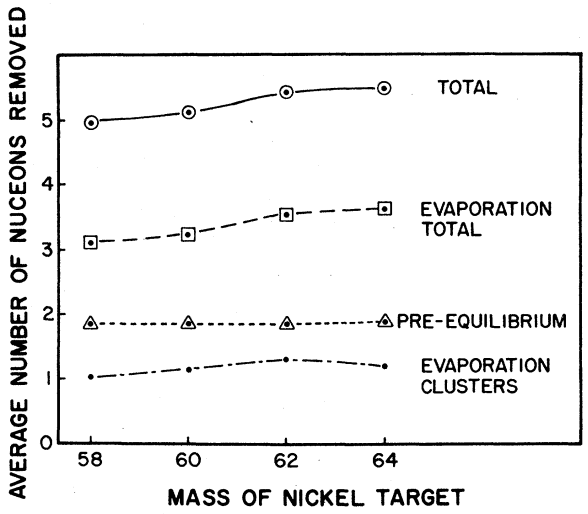

FIG. 11. Partitioning of nucleon removed between the pre-equilibrium and equilibrium phases as predicted by the cascade model for 0 proton energy of 136 MeV.

emitted in the equilibrium phase; of the latter, two are emitted as nucleons and the third is emitted in the form of clusters such as d, t, ^{3}He, and ^{4}He. (2) All of the models predict that beyond 100 MeV bombarding energy the fraction of the initial interactions which leads to emission of at least one fast nucleon is essentially 100%. At 50 MeV this fraction is still large, 60–80%, although actual values vary with the type of model calculation. (3) The energy dependence of the average number of nucleons emitted in the pre-equilibrium phase as predicted by the cascade model, shown in Fig. 12, has a slope of 0.007 nucleons per MeV. When compared to the observed value of 0.015 nucleons per MeV one can conclude that there is a small increase in the number of nucleons emitted in the evaporation phase with energy or, in other words, the average excitation energy of the equilibrium phase slightly (~5 MeV) increases over 80–160 MeV incident proton energy. (4) Calculations reveal that the range of excitation energy that a nucleus is left in after pre-equilibrium emission is very broad, with noticeably greater probability for lower excitations; for example, for the case (see Fig. 13) of 136 MeV protons on ^{58}Ni, $A=58$ nuclei are left excited over a range of 0–130 MeV, $A=57$ nuclei are left with 0–120 MeV excitation, and so on. An experimental study of this phenomenon through particle-gamma coincidence studies may provide a stringent test of the models and may reveal their limitation a little more explicitly. (5) The average energy of nucleons emitted in the pre-equilibrium phase is calculated to decrease precipitously after the first emission, e.g., at 136 MeV the first nucleon is emitted with an average energy of about 50 MeV, but with two or more encounters this value drops to between 10–20 MeV. A particle multiplicity measurement may provide a good test for this aspect of the model dynamics.

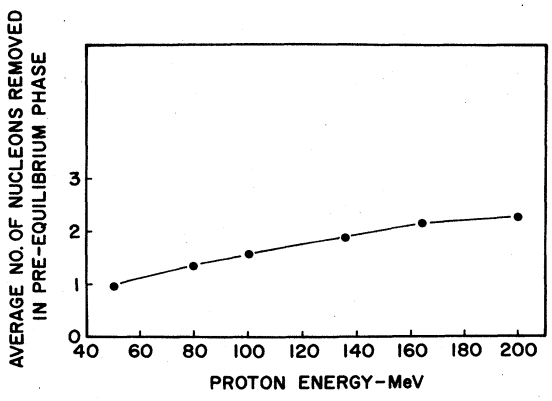

FIG. 12. Average number of nucleons emitted in the pre-equilibrium phase predicted by the cascade model as a function of the incident proton energy for ^{58}Ni.

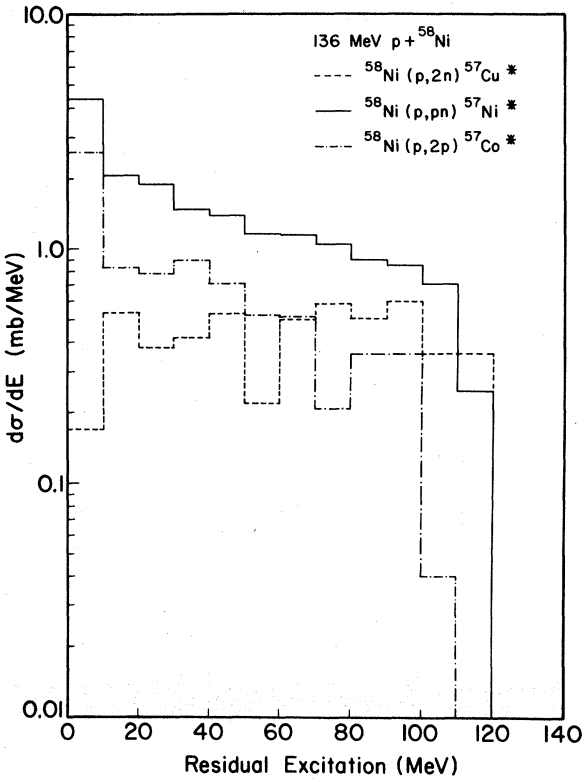

FIG. 13. The excitation energy range of nuclei which are one nucleon removed from the ^{58}Ni target nucleus predicted by the cascade model for incident proton energy of 136 MeV.

Some recent arguments in the literature pertaining to mean free paths (λ) of nucleons in nuclear matter are also worthy of some attention. In searching for answers to phenomena pertaining to the equilibrium process, Gadioli *et al.*[23,24] presented arguments that a mean free path for 20 to 100 MeV nucleons in nuclear matter of the order of 16.7 fm, instead of the value of about 4.2 fm obtained from using the free nucleon interaction cross sections in a Fermi gas model calculation, gives a better account of the energy spectra of emitted protons. On the other hand, Blann[25] claimed that an error in the formulation of Gadioli's exciton model necessitates an increase in the assumed mean free path.

The qualitatively good agreement of the calculations in terms of the hybrid model with the present results indicates that large modification of the calculated mean free path is not necessary, at least not by a factor of 4. The factor of 2 used in most EVAHYB calculations was found to be necessary to simulate the effects of the nuclear surface on the emission process. Even this factor of 2 was not found to be necessary at 80 MeV when the results of the geometry-dependent-hybrid (GDH) model,

which incorporates surface effects, were compared with experiment. It is significant, though, that a drastic (factor of 2) increase in the assumed mean free path is required to change $\langle \Delta A \rangle$ by approximately the same amount that GDH changes this quantity in comparison to the simple hybrid model at 80 MeV. It is plausible that much of the increase in the mean free path in Refs. 24 and 25 is necessitated by the non-inclusion of these surface effects.

As noted above, similar studies of nuclide production have been made for medium energy pions, $E_\pi \leq 200$ MeV, interacting with nickel isotopes. One of the important differences between the proton-induced and pion-induced reactions is that whereas with pions, e.g., on a ^{62}Ni target, the product mass spectrum peaks[26] at $A = 54-56$, with protons after the initial increase the production cross sections fall off more or less smoothly as the number of nucleons removed increases. In particular VEGAS plus evaporation calculations show[26] important qualitative deviations from the observed pion-induced mass spectra. The fact that this model satisfactorily reproduces the proton-induced spectra indicates that there is some extra physics in the pion-nucleus reaction that is not embodied in the VEGAS code.

In closing it is sufficient to say that systematic data of other kinds such as energy spectra of emitted particles, the particle multiplicities, and particle-gamma coincidence are needed in order to answer some of the questions that are raised here.

ACKNOWLEDGMENTS

This research work has been supported in part by grants from the National Science Foundation. We are thankful to Professor M. Blann of Rochester University for many discussions and for providing various hybrid model codes and to Dr. J.N. Ginocchio of the Los Alamos Scientific Laboratory for making the VEGAS code available to us.

APPENDIX: INPUT PARAMETERS FOR MODEL CALCULATIONS

There are several possible combinations of input parameters that can be used for ALICE, EVAHYB, VEGAS, and DFFMH. The ones used in this work are given below.

1. Hybrid model calculations

For single pre-equilibrium model calculations the GDH model in ALICE was used. All default input parameters were used, except the following:

(a) Experimental masses were used to determine the binding energies instead of the mass formula. Pairing was removed from the calculated binding energies in the same way that would be done if the option for shell corrected masses, zero pairing were used (default option).

(b) Inverse cross sections for ^{59}Co were used. These were calculated from the optical model by ALICE subroutines using the parameters given by Perey and Perey.[27]

(c) Reaction cross sections from VEGAS (see Table VI) were used so that all calculations would be normalized to the same total cross section.

(d) Weisskopf evaporation was used.

(e) Initial exciton number = 3.0. Initial excited neutron number = 0.8. Initial excited proton number = 1.2.

(f) Nucleon-nucleon mean free paths were used. The mean free path multiplier was 1.0.

For multiple pre-equilibrium calculations the computer code EVAHYB was used. Some modifications were introduced into the code. These included extension of the dimensions to obtain cross sections for nuclei farther away from the target, separate accumulations of the pre-equilibrium and evaporation particle spectra, plotting routines, and output options. All default parameters were used, with the exception of:

(a) Reaction cross sections from VEGAS were used (Table VI).

(b) Initial exciton number = 3.0. Initial excited neutron number = 0.8. Initial excited proton number = 1.2.

(c) Mean free paths derived from free nucleon-nucleon scattering were used. A mean free path multiplier of 1.0 or 2.0 was used and is so denoted when an EVAHYB calculation is referenced.

(d) The same inverse cross sections as described above with GDH were used. These were also used in the VEGAS plus ALICE calculations described below.

2. Cascade model calculations

The computer code VEGAS was used for the pre-equilibrium cascade model calculations. The number of cascades run was 8000–10 000 for each case. Relevant input parameters for the calculations presented in this work are:

(a) The cutoff energies for neutrons and protons, respectively, were the binding energy of the last neutron in the target and the binding energy of the last proton plus the Coulomb energy. Nucleons with energies below these values are considered to be captured. The actual values of these cutoffs

were in (MeV):

Target	^{58}Ni	^{60}Ni	^{62}Ni	^{64}Ni
Neutron	12.2	11.4	10.6	9.7
Proton	14.2	15.6	17.4	19.0.

(b) No reflection or refraction was included at the potential boundaries. This option was chosen since in previous work inclusion of reflection and refraction resulted in poorer comparisons with the data, indicating that this effect is overestimated in the calculation.

(c) No restriction on the distance between successive collision sites was used.

The input parameters for DFFMH followed the suggested options. The maximum of six particles n, p, d, t, ^{3}He, and α were allowed in the evaporation phase. The parameter a in the level density expression $\rho(U)\alpha e^{2\sqrt{aU}}$ was taken to be $A/20$ where A is the mass number of the evaporating system. Inverse cross sections are calculated internally using "continuum theory" by DFFMH with no available input parameters for modification.

ALICE calculations used inverse cross sections from a ^{59}Co evaporating system for all targets. A Co nucleus was thought to be more typical of the evaporating nuclei than a Cu nucleus. The differences between the cross sections for formation of different Co nuclei are mostly geometrical, an effect that changes the emission probabilities of all particles in the same direction and roughly preserves the relative probability of evaporating a particle of a given type. Thus, the ^{59}Co system was chosen and used for all ALICE calculations even though the nucleus cannot be formed with a ^{58}Ni target. The optical model parameters were the same as given above.

---

*Present address: LAMPF, Los Alamos Scientific Laboratory, M.S. 831, Los Alamos, N. M. 87545.
†On leave from INR, Swierk, Poland.
‡Present address: Argonne National Laboratory, Argonne, Ill.

[1]M. Sadler, J. Jastrzebski, A. Nadasen, P. P. Singh, L. L. Rutledge, Jr., T. Chen, and R. E. Segel, Phys. Rev. Lett. 38, 950 (1977).
[2]J. Jastrzebski, H. Karwowski, M. E. Sadler, and P. P. Singh, Bull. Am. Phys. Soc. 22, 634 (1977); and to be published.
[3]J. Wiggins, P. P. Singh, M. Sadler, H. Karwowski, J. Jastrzebski, and D. G. Sarantites, Bull. Am. Phys. Soc. 23, 626 (1978) and to be published.
[4]R. E. Segel, T. Chen, J. V. Maher, J. Wiggins, M. E. Sadler, P. P. Singh, and P. T. Debevec, Bull. Am. Phys. Soc. 23, 926 (1978); and to be published.
[5]P. D. Barnes, R. A. Eisenstein, W. C. Lam, J. Metler, R. B. Sutton, M. Ecklause, J. Kane, R. E. Welsh, D. A. Jenkins, R.J. Powers, R. Kunselman, R. P. Redwine, R. E. Segel, and J. P. Schiffer, Phys. Rev. Lett. 29, 290 (1972).
[6]H. E. Jackson, L. Meyer-Schutzmeister, T. P. Wangler, R. P. Redwine, R. E. Segel, J. Tonn, and J. P. Schiffer, Phys. Rev. Lett. 31, 1353 (1973).
[7]V. G. Lind, H. S. Plendl, H. O. Funsten, W. J. Koseler, B. J. Lieb, W. F. Lankford, and A. J. Buffa, Phys. Rev. Lett. 32, 479 (1974).
[8]D. Ashery, M. Zider, Y. Shamai, S. Cochavi, M. A. Moinester, A. I. Yavin, and J. Alster, Phys. Rev. Lett. 32, 943 (1974).
[9]H. Ullrich, E. T. Boschitz, H. D. Engelhardt, and C. W. Lewis, Phys. Rev. Lett. 33, 433 (1974).
[10]C. C. Chang, N. S. Wall, and Z. Fraenkel, Phys. Rev. Lett. 33, 1493 (1974).
[11]H. E. Jackson, D. G. Kovar, L. Meyer-Schutzmeister, R. E. Segel, J. P. Schiffer, S. E. Vigdor, T. P. Wangler, R. L. Burman, D. M. Drake, P. A. M. Gram, R. P. Redwine, V. C. Lind, E. N. Hatch, O. H. Otteson, R. E. McAdams, B. C. Cook, and R. B. Clark, Phys. Rev. Lett. 35, 641 (1975).
[12]M. E. Sadler, Ph.D. thesis, Indiana University, Bloomington, Indiana (1977); IUCF Internal Report No. 77-2.
[13]M. Blann, Annu. Rev. Nucl. Sci. 25, 123 (1975) and references therein.
[14]N. Metropolis, R. Bivias, M. Storem, A. Turkevich, J. M. Miller, and G. Friedlander, Phys. Rev. 110, 185 (1958).
[15]K. Chen, Z. Fraenkel, G. Friedlander, J. R. Grover, J. M. Miller, and Y. Shimamoto, Phys. Rev. 166, 949 (1968).
[16]V. S. Barashenkov, H. W. Bertini, K. Chen, G. Friedlander, G. D. Harp, A. S. Iljinov, J. M. Miller, and V. D. Toneev, Nucl. Phys. A187, 531 (1972).
[17]M. Blann, OVERLAID ALICE, Report No. COO-3494-29 (1975).
[18]M. Blann and J. Bishplinghoff, Hybrid Code Description, Report No. COO-3494-27 (1975).
[19]A. Mignerey, and M. Blann (unpublished).
[20]I. Dostrovsky, Z. Fraenkel, and G. Friedlander, Phys. Rev. 116, 683 (1959).
[21]V. F. Weisskopf and D. H. Ewing, Phys. Rev. 57, 472 (1940).
[22]J. R. Wu, C. C. Chang, H. D. Holmgren, N. S. Wall, J. P. Didelez, and C. Butterfield, in *Proceedings of the Second International Conference on Clustering Phenomena in Nuclei, College Park, Maryland, 1975,* edited by D. A. Goldberg, J. B. Marion, and S. J. Wallace (National Technical Information Service, Springfield, 1975), VA.6, p. 1.
[23]E. Gadioli, E. Gadioli Erba, G. Tagliaferri, and J. J. Hogan, Phys. Lett. 65B, 311 (1976).
[24]E. Gadioli, Nukleonika 21, 385 (1976).
[25]M. Blann, Phys. Lett. 67B, 145 (1977).
[26]H. E. Jackson, S. B. Kaufman, D. G. Kovar, L. Meyer-Schutzmeister, K. E. Rehm, J. P. Schiffer, S. L. Tabor, S. E. Vigdor, T. P. Wangler, L. L. Rutledge, Jr., R. E. Segel, R. L. Burman, P. A. M. Gram, R. P. Redwine, and M. A. Yates-Williams, Phys. Rev. C 18, 2656 (1978).
[27]F. G. Perey and C. M. Perey, At. Data Nucl. Data Tables 13, 294 (1974).